

Validation of a Thermoplastic Composite Material Model for Low Carbon Vehicle Applications

Oliver Tomlin (GRM Consulting Ltd), Neil Reynolds (WMG, University of Warwick)

1 Abstract

The methods developed for creating and validating a thermoplastic composite (TPC) material model in LS-DYNA are presented. Included are details of the mechanical characterisation methods and test types required to fulfil the input requirements of MAT058. Model input data are validated through correlation between coupon and sub-system physical tests and simulations with justification of the boundary conditions. The test methods are explored in more detail following the sub-system model validation, giving a clear understanding of the need for integration between CAE and test. Validation of the material model is further explored with results from quasi-static and impact tests. Results show that confidence in the predictive capabilities of MAT058 is high.

2 Introduction

2.1 Vehicle light-weighting and composites

Legislative targets defined in order to reduce environmental impacts arising from road vehicle usage have led to a focus on research into alternative propulsion technologies and aggressive vehicle light-weighting solutions. Considering that kerb weight reductions improve fuel efficiency and therefore the CO₂ emitted per kilometre travelled, vehicle light-weighting has become a critical theme for the UK's New Automotive Innovation & Growth Team (NAIGT) strategy. This roadmap establishes an industry-led short- and medium-term research approach to deliver lightweight structures and functional integration of parts.

One study has found that the average fuel reduction factor for a range of conventional light-duty internal combustion engine (ICE) platforms is 0.69 l/100 km for every 100 kg of weight saved [1]; other work found that a total vehicle mass reduction of approximately 15% could result in a 10% decrease in fuel consumption and consequently CO₂ emissions [2].

Best-in-class steel body-in-white (BIW) structures constitute approximately 15-25% of a vehicle's total mass and approximately 10-15% for aluminium-based vehicles [3]. Therefore the BIW and associated continuous load-bearing structural elements are an obvious focus for mass-reduction engineering. The substitution of traditional metallic structures with high performance composite materials can greatly assist in meeting aggressive weight reduction targets. Recent research has indicated that mass reductions of >40% are achievable when using composites, leading to total vehicle weight savings of approximately 20% [4].

2.2 Low Carbon Vehicle Technology Programme

An experimental case study investigating the use of TPCs for automotive primary structures was carried out at WMG as part of the ERDF-AWM funded Low Carbon Vehicle Technology Programme (LCVTP). The purpose of LCVTP was to develop and deploy technology and skills across the automotive supply chain in the UK West Midlands region, accelerating the introduction of low carbon technologies into the automotive industry, in line with the NAIGT strategy. A broad programme of research and development covered 15 work streams of activity.

The *lightweight structures* work stream primary objective was to develop materials and process technologies suitable for application in vehicle structures to support a predicted weight saving of at least 20% over conventional (e.g. metallic) materials process technology. Technologies investigated needed proving to a concept-level, and a range of individual tasks were formulated within the work stream to deliver the information and data to achieve this. The topics of material selection, process development, CAE simulation tool development, component performance, and the economic aspects and environmental impact associated with material substitution were investigated. GRM Consulting was engaged to carry out development and validation of CAE tools to advance the application of the chosen materials.

3 Materials

In order to support high volume manufacturing processes relevant to the mainstream automotive industry (>50,000 units per annum), a thermoplastic composite laminate material was selected. Specifically, a laminate based on unidirectional glass fibre reinforced polyamide 6 extruded tape (PA6-GF60) was chosen [5]. The unidirectional glass fibre ply architecture offered ideal performance whereby plies could be aligned exactly according to applied loads whilst the fibre configuration possesses zero crimp (the out-of-plane deviation of the fibres typically present in a woven reinforcement architecture that decreases the in-plane mechanical performance of a laminate). Additionally, regarding cost, it was considered important to select a high performance composite that was based on widely available and correspondingly economical constituents such as an engineering polymer (PA6) and E-glass fibre. Finally, PA6 provides a good portfolio of desirable properties in terms of toughness/ductility, manufacturing processability to support short cycle times and thermal resistance, having a melt temperature between 225 – 230°C.

4 Manufacturing

Two separate manufacturing processes were used for the production of test material at WMG from the PA6-GF60 TPC laminate material: vacuum bagging and rapid hot stamp forming. Vacuum bagging was used to manufacture flat plaques from which coupon-level test specimens could be subsequently machined. TPC laminate plaques were laid-up using a continuous glass reinforced extruded PA6 tape and processed at 235°C at 0.9 bar in a vacuum bag contained within a hot air oven.

A novel rapid hot stamping process was used to manufacture sub-system physical test components. The test component was selected as a closed “Top-Hat” section box-beam, representative of an automotive front longitudinal section or a side impact beam, Figure 1.

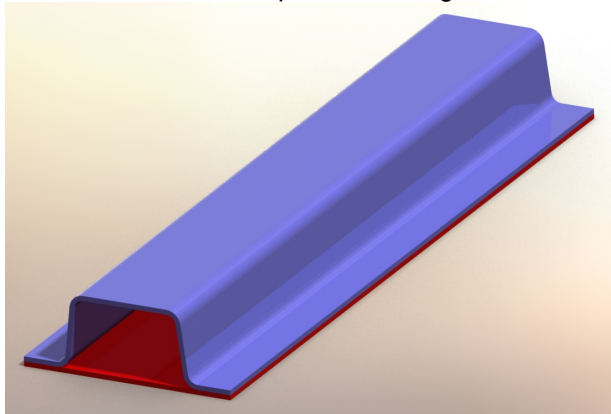


Figure 1: LCVTP U-channel rendered model (approximately 40mm x 70mm x 450mm)

The hot-stamping process was implemented on a 100 tonne vertical clamp compression moulding press using purpose-made oil-heated matched steel tooling. 16-ply (3mm thick) laminate pre-forms were assembled by hand using a generic non-optimised cross-ply 0-90 stacking sequence, where the 0° datum was in line with beam length. The TPC laminate pre-forms were heated to 235°C and manually transferred to the heated tool (120°C) for stamp-forming at 10 MPa (100 bar). The time between loading the pre-heated blank into the open tool and de-moulding the part was 60 seconds.

The beams with closures were assembled in a manner that mimicked standard automotive assembly processes. After stamping, the beams were trimmed using CNC water-jet cutting with 3mm closure plates (identical lay-up to the moulded beam) joined to the composite via a hybrid joining process using adhesive and mechanical fixings. Single-part structural epoxy was applied and the uncured assembly was mechanically joined using a self-piercing rivet (SPR) process. Finally, the assembled uncured parts were put in an oven that was programmed to replicate the automotive BIW paint-bake cycle, whereby the 1K epoxy adhesive would heat-cure.

For dynamic axial crush testing, the 450mm beams were shortened to 375mm to stabilise the crush column and prevent global buckling failure modes. Failure initiators were introduced onto the beam ends to ensure that a stable and progressive crush mode occurred in each test. The beams had a 1mm-wide notch cut at 45° into each of the upper ‘top-hat’ radii, 10mm from the contact end of the beam.

5 FEA approach and testing

The approach taken to develop the robust FEA models for predicting the performance of TPC laminate components is shown in Figure 2.

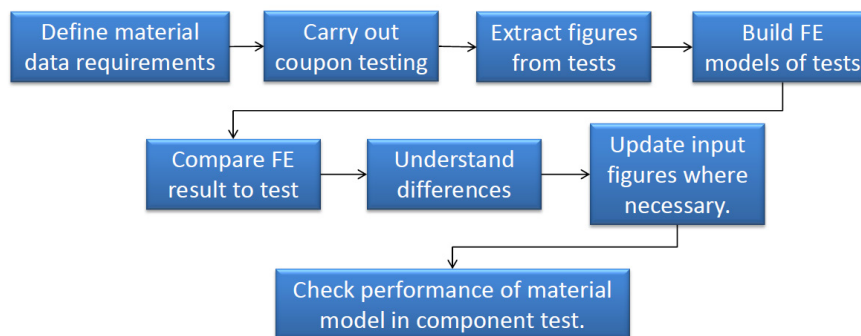


Figure 2: Step-wise approach to FEA model development, GRM Consulting Ltd

5.1 Material card selection and input data

The MAT058 model was selected as it can be used in the creation of multi-ply laminate models made from individual unidirectional plies [6], and it can also represent non-linear stress-strain behaviour such as the in-plane bilinear shear response [7], as shown in Figure 3.

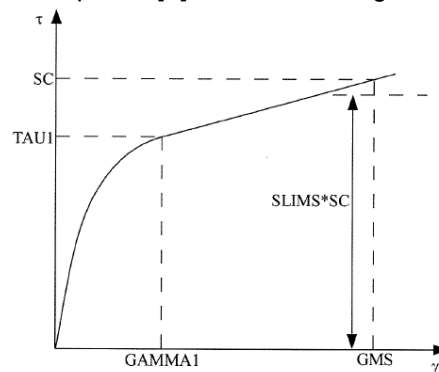


Figure 3: Shear stress-shear strain schematic from MAT058 guide [6]

The key input data requirements for MAT058 could be summarised as the elastic material constants, ultimate stress limits, and the strain/stress values describing the onset of non-linearity for off-axis loading – the values generated from coupon testing are displayed in Table 1.

Test type	Values	Description
UD ply Tension 0°	$E_A, \nu_{AB}, E_{11T}, X_T$	Young's modulus, Poisson's ratio, strength
UD ply Tension 90°	$E_B, \nu_{BA}, E_{22T}, Y_T$	Young's modulus, Poisson's ratio, strength
Shear (in-plane), $\pm 45^\circ$ tension test	$G_{AB}, T_1, \gamma_1, SC, GMS$	Shear modulus, shear strength, onset of non-linearity
Shear (out-of-plane), short beam flexion	$G_{CA} (\approx G_{BC}), SC$	Shear modulus

Table 1: MAT058 input data

Note that several estimations were necessary and the quantities in Table 1 do not constitute the entire input deck – due to time constraints, compressive testing was not possible, and interlaminar testing in the y-z plane was not experimentally practical, requiring a machined laminate block in excess of 80 plies thick.

5.2 Mechanical testing – coupon level

All coupon-level testing was conducted on a screw driven 100kN Instron 5800R. Biaxial contacting extensometry was used to obtain axial and transverse strain and hence Young's modulus and

Poisson's ratio, and the in-plane shear properties. In the case of out-of-plane shear testing, 1.3M GOM ARAMIS 2D digital image correlation (DIC) was used to capture the through-thickness shear angle of the deflected beam.

5.2.1 UD ply, 0° and 90°

Static tensile tests were carried out on uni-directionally reinforced material according to ASTM D3039 at room temperature [8]. Testing was done on UD stacks to ascertain the properties at individual ply level, as the performance should be equivalent. The individual specimen size for UD 0° testing was 250 x 15 x 1.1mm (5 plies thick), rectangular samples with integral tabs made using 90° plies located only in the gripping area, leading to ply drop-offs into the gauge region. The specimen size for 90° testing was 225 x 25 x 2.2mm (10 plies thick), rectangular samples with no tabs.

5.2.2 In-plane shear properties

G_{AB} (in-plane ply shear modulus) was measured using static tensile testing on a $\pm 45^\circ$ laminate according to ASTM D3518 [9]. Tests were carried out on material 16 layers thick, laminated at $(0/90)_{4S}$ and machined at 45° to the 0° datum. The testing was carried out with bi-axial contacting extensometry recorded to enable the calculation of shear strain. The specimen size was 250 x 25 x 3.52mm, rectangular samples with no tabs.

5.2.3 Out-of-plane shear properties

G_{CA} was measured using static 3-point bend testing according to ASTM D2344 [10], a standard generally used only for measuring interlaminar shear strength (ILSS). Although the standard doesn't discuss the calculation of shear modulus values, a method has been suggested that can provide an estimate [11]. To obtain the shear modulus, 2D DIC was used to record the shear angle on the side surface of the beam along the neutral axis (Figure 4), and was plotted against apparent shear stress. The shear modulus was calculated as the derivative of the linear portion of this curve.

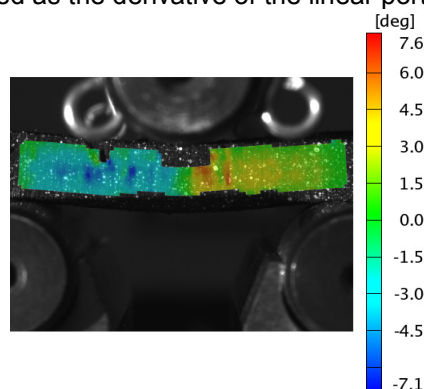


Figure 4: Short beam shear angle measurement from 2D DIC technique, WMG

Short-beam flex specimens were cut from a $(0)_{28}$ laminate ~6mm thick. The specimens were 40 x 12 x 6mm in size, loaded in 3-point bend at an outer span of 24mm (4 x h). Transverse shear properties were not measured, and instead it was assumed that the transverse shear properties were approximately equal to the out-of-plane shear properties ($G_{BC} \approx G_{CA}$).

5.3 Mechanical testing – sub-system (component) level

The quasi-static 3-point flexure tests were conducted on a 250kN Dartec servo-hydraulic test frame with a 400mm outer beam span at 20mm/minute (0.333mm/s) up to a maximum deflection of 50mm. Load-deflection curves were recorded for each test.



Figure 5: 3-point Flexure Test Setup

The dynamic axial crush (impact) tests were carried out on a fully instrumented purpose-built spring assisted Instron drop weight impact test machine. 8 kJ of kinetic energy was applied at a speed of 15.2 m/s at impact. Load-time and impact speed were recorded along with high-speed digital photography to capture failure initiation and progression.

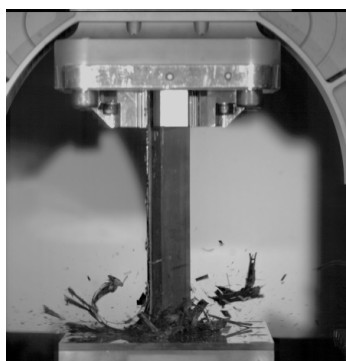


Figure 6: Impact Test Example

6 Experimental results

6.1 Results - static tensile coupon-level

The UD ply tested in the 0° direction had an average Young's modulus and a tensile strength of 28 GPa and 730 MPa respectively. The UD ply loaded at 90° to the fibre alignment had an average Young's modulus of 6.79 GPa and an average tensile strength of 39 MPa. Table 2 gives the summary tensile data extracted from the static tensile test series as used in the MAT058 input deck.

Tensile properties	Symbol	Units	Mean	Std Dev
Young's Modulus 0°	E_a	GPa	28.65	1.27
Young's Modulus 90°	E_b	GPa	6.79	0.66
Major Poisson's Ratio	ν_{AB}	□	0.38	0.04
Minor Poisson's ratio	ν_{BA}	□	0.08	0.01
Ult. Tensile Strength 0°	XT	MPa	732.64	27.55
Ult. Tensile Strength 90°	YT	MPa	38.59	1.08
Ult. Tensile Strain 0°	E11T	□	0.022	0.001
Ult. Tensile Strain 90°	E22T	□	0.006	0.001
Density	RO	g/cc	1.72	n/a

Table 2: Static tensile data for PA6-GF60, WMG

6.2 Results - static shear coupon-level

Representative static coupon shear behaviour and extracted mean results are shown in Figure 7 and Table 3 respectively.

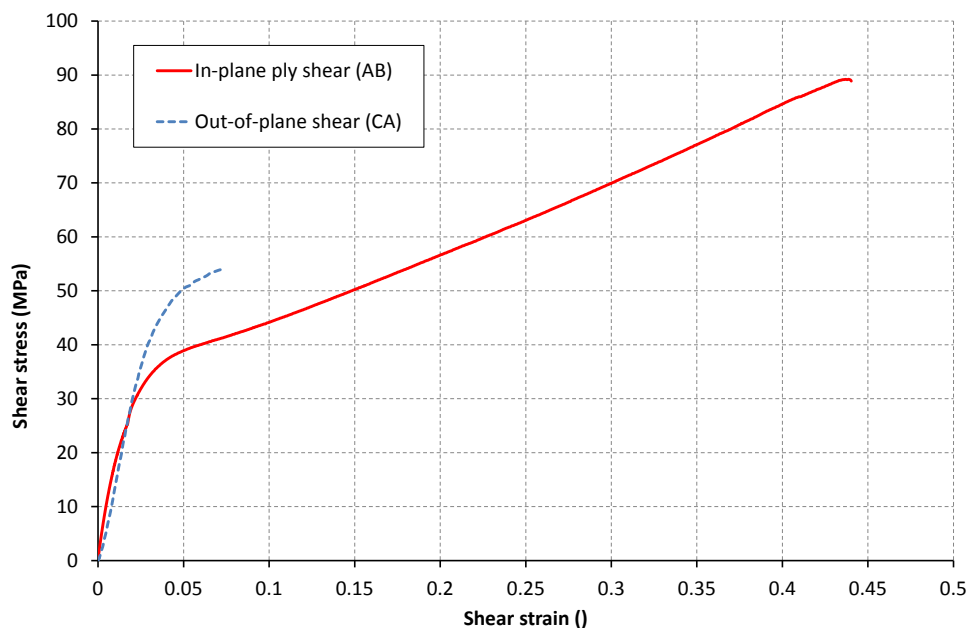


Figure 7: Static shear performance of PA6-GF60 material, WMG

Shear properties	Symbol	Units	Mean	Std Dev
In-plane shear modulus	G_{AB}	GPa	2.08	0.20
In-plane shear stress limit	TAU1	MPa	41.34	-
In-plane shear strain limit	GAMMA1	̵	0.0625	-
In-plane shear strength	SC	MPa	90.76	14.30
Ult. in-plane shear strain	GMS	̵	0.44	0.03
Out-of-plane shear modulus	G_{CA}	GPa	0.99	0.09

Table 3: Static shear data for PA6-GF60 material, WMG

7 FEA model development

7.1 Coupon Calibration

The material parameters recorded from the coupon testing were used in their entirety as initial inputs to the MAT058 material model. Where details were not available estimates were made from published data for the PA6-GF60 material. Using realistic values was quickly proven to be a key part of obtaining a reliable model, which delivered the expected performance in single-axis stress states. Coupon boundary conditions were shown to control the onset of failure and when corrected, an outstanding correlation with the test data was observed.

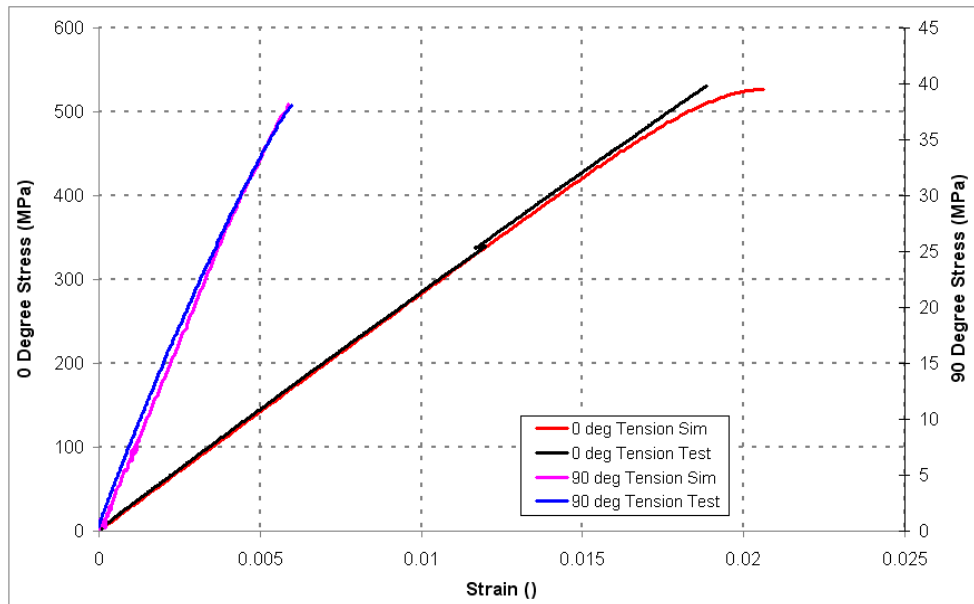


Figure 8: 0 and 90 Degree Coupon Calibration

The sensitivity of the material model in stiffness and strength was assessed against various element sizes and it was shown to be insensitive between 2mm and 8mm edge lengths.

7.2 Coupon Observations

By starting the material calibration with a coupon test, the fine details of the material model and its behaviour could be observed. This gave a far more detailed understanding of performance during the following component calibration exercises. In particular the parameters that were fully explored by the coupon work could be fixed and did not require later investigation. All test methods were calibrated in great detail, except for the in-plane shear model. Using the results from the testing and following the relevant guidance described in Figure 3, the model showed excellent pre “yield” correlation, with a significant strength and stiffness reduction post “yield”, Figure 9.

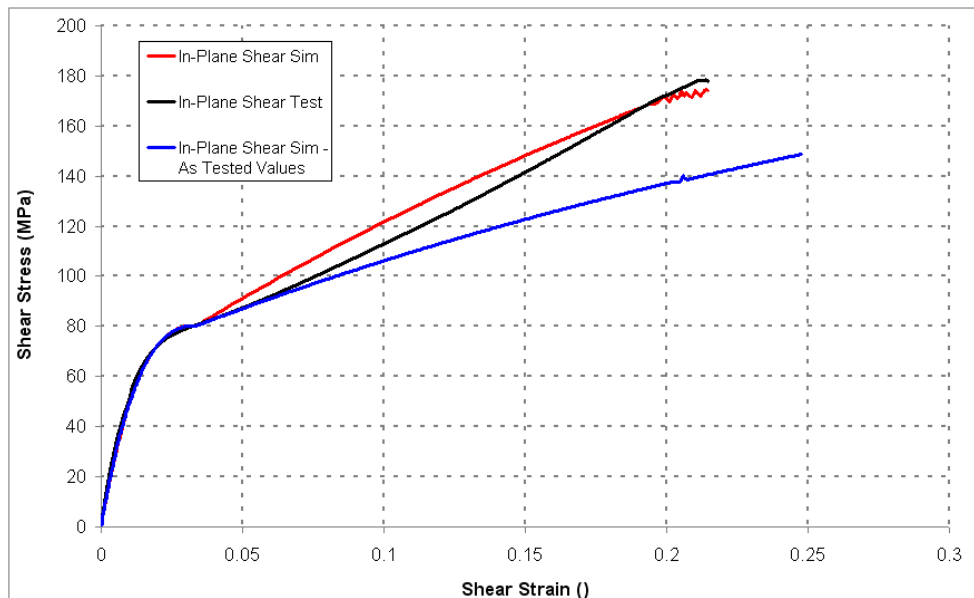


Figure 9: In-Plane Shear Calibration

The reduced post “yield” stiffness has also been observed in latter calibration of a woven carbon-epoxy material. The material parameters SC and GMS can be easily modified by 17% to bring a satisfactory correlation, however the justification for this is not clear. Research into the methods of testing in-plane shear show that some strength reduction is observed with the +45 coupon test when

compared to the ideal situation of a fully formed +-45 tube test [12]. However, given that MAT058 has been defined specifically to utilise this test result, this reduction is likely to have already been taken into account. It is reassuring to observe that only a small percentage of our plies are likely to be working in the post “yield” region of pure in-plane shear. This has been verified during our impact work where no change in the simulation results has been noted when this parameter was modified.

7.3 3 Point Bend Calibration

Using the calibrated MAT058 material model as a direct input to the 3-point bend calibration produced initially disappointing results. As has been shown before, the correct compensation for true test boundary conditions was vital to improving the performance and not using the assumed inputs. In particular the spring-back of the sample post-manufacture had the greatest influence on the calibration. However, these updates were unable to compensate for a reduction in stiffness at 30% of the total deflection. With all the boundary conditions explored, this left only the material card to modify. The parameters which were uncalibrated from the coupon testing were the compression properties as these were necessarily sourced from published data.

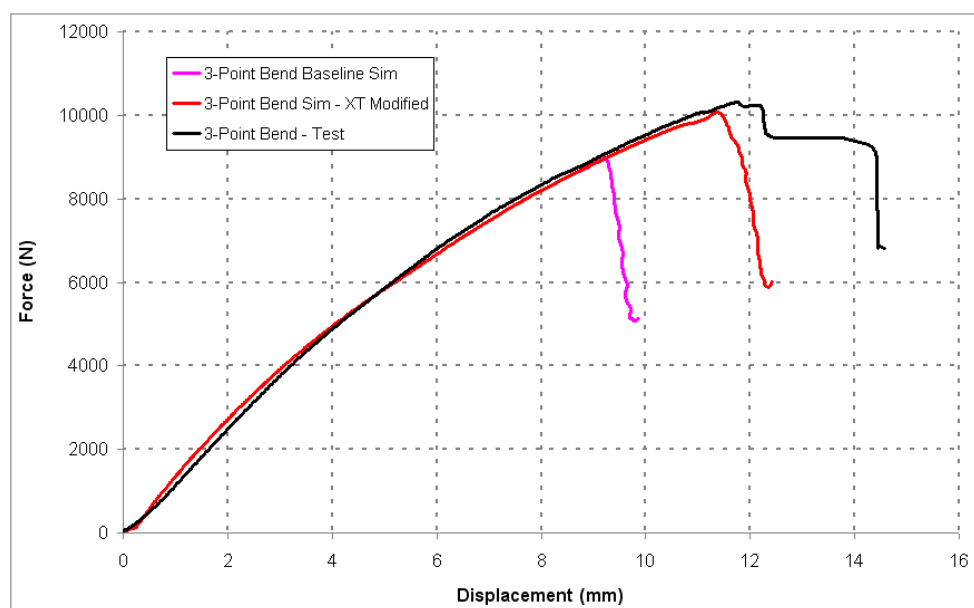


Figure 10: 3 Point Bend Calibration.

Modification of the compression strength and strain quickly determined the most suitable inputs, however the peak strength still fell short of the test. Sensitivity studies demonstrated that this was entirely controlled by the X direction tensile strength, but given that this was a calibrated parameter there was little justification to make changes. On utilising the rule of mixtures (Equation 1) to estimate the tensile strength, the value was found to match very closely that required to gain calibration to the test result.

Equation 1, Rule of mixtures:
$$\sigma_c = \sigma_m * V_m + \sigma_f * V_f$$

This gave more weight to the hypothesis that the coupon test had produced an unrealistically low tensile strength. In collaboration with the material testing colleagues, the coupon size and end conditions were modified and repeating the tests gave much improved results. These matched closely the strength predicted by the FE model and the rule of mixtures and gave confidence in the quality of this calibrated model.

7.4 3 Point Bend Observations

It was demonstrated by the 3 point bend calibration work that the initial material model was working very well. However, the value of carrying out this test with fixed and known boundary conditions has

been clearly shown. The ability to explore the material parameters which had not been calibrated and to verify the complete model resulted in a very high quality result. An unexpected benefit was the resulting collaboration between the test laboratory and simulation team and it is to be expected that this will continue to be necessary with new materials. A feed-back loop between the two should always be planned and allowed for. The 3 point bend calibration has shown that MAT058 in this scenario gives a superb level of accuracy.

8 Box-beam Impact

The final assessment of the calibrated MAT058 material model was an impact test in laboratory conditions. The 8kJ impact described previously was represented in the FE model, with accurate replication of the boundary conditions. This required the clamping system to be modelled in some detail to ensure that the first loading of the sample was captured. The composite was represented by 16 plies, each being 0.22mm thick using the *PART_COMPOSITE definition, with orientations matching the manufactured component.

The first model results showed buckling and plasticity inconsistent with a composite material. With all material parameters proven from the coupon and 3 point bend test, this left the ERODS and SOFT inputs as the only valid exploration. Research has shown that these two parameters work in conjunction with each other and allow for the crush and pulverisation behaviour associated with impact events to be modelled correctly. It is our observation that they are “tuning” parameters with little real-world input. Deletion of distorted elements with high plastic strain can be achieved by ERODS or TSIZE. However, TSIZE is a backup plan for highly deformed elements, which by that point should be carrying little load.

ERODS defines the maximum effective strain for element layer failure. In MAT058, the scalar strain quantity which is evaluated against the failure strain ERODS is computed at each integration point, from the two in-plane normal strains and the in-plane shear strain using the following equation [13]:

$$\text{Equation 2, ERODS: } \frac{2}{\sqrt{3}} \times \sqrt{\left[3 \times \left(\frac{eps1 + eps2}{2} \right)^2 + \left(\frac{eps1 - eps2}{2} \right)^2 + eps4^2 \right]}$$

When the effective strain at an integration point exceeds ERODS, that integration point fails and carries no more stress. The element is only deleted when all integration points have failed. In conjunction with ERODS, the SOFT parameter reduces the strength of elements sharing nodes with those that have already been deleted. This effect is controlled by the “crashfront” algorithm and it is clear that SOFT will have no effect if there is no element deletion as a result of ERODS.

Our work has shown that it is advisable to use a very small value for TSIZE. This prevents any conflict between it and ERODS and also ensures that element deletion and component failure are controlled by ERODS and SOFT alone.

Following a process of iteration and investigation for the ERODS and SOFT parameters, the calibration results shown in Figure 11 were achieved.

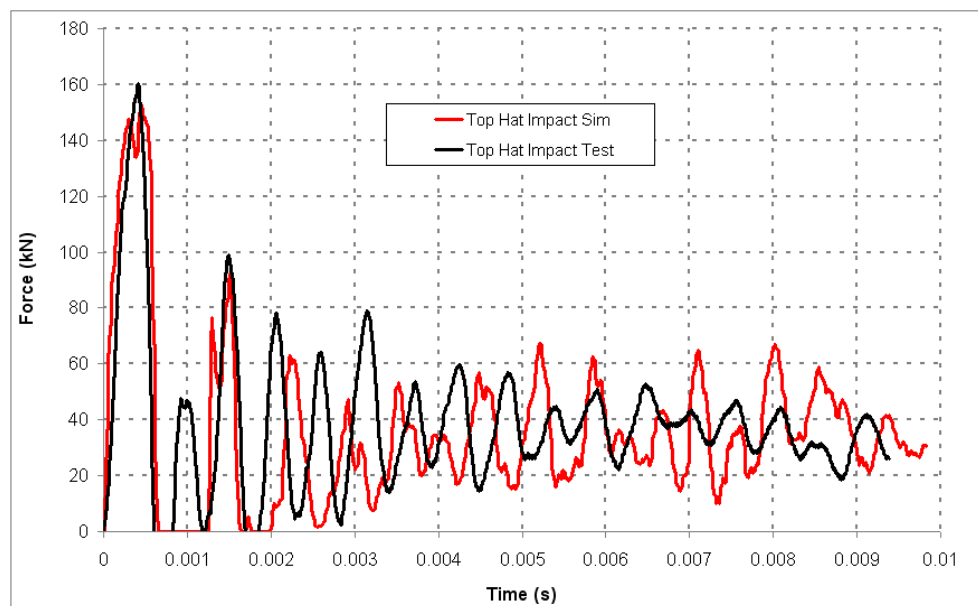


Figure 11: Impact Calibration Force versus Time

These results demonstrate an outstanding level of correlation, with the first peak and the load level when stable crush has been reached matching well. This is equivalent to what can be achieved with steel components in similar scenarios. A visual comparison, as shown in Figure 12, demonstrates an equally high level of confidence, with the corner failure and closer peel matching between test and simulation.

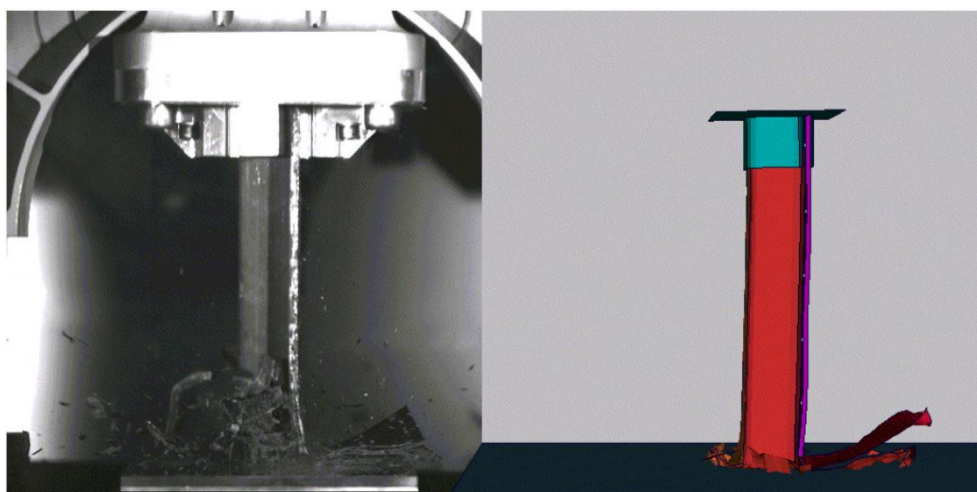


Figure 12: Impact Calibration Comparison

9 Summary

The work presented here has shown the power of MAT058 when the opportunity is taken to carry out a full calibration exercise from small scale up to impact components. It has also demonstrated that the regular communication between test and simulation teams is advantageous when creating models of advanced materials. Understanding how the material card works and the interaction between parameters must be noted before any attempt is made to undertake calibration and certainly before full-scale impact analyses. Using LSTC implemented material cards offers a level of robustness not usually associated with the newest developments.

Unfortunately, exploration in other loading regimes has shown that the quality of calibration is entirely controlled by ERODS and SOFT. It is observed that these parameters are loading specific, which is highly undesirable. An ERODS value of 0.1 was required at low strain rates with a value of 0.8 required at higher strain rates.

10 Acknowledgements

The work carried out in this paper constituted a part of the research in Work Stream 7 of the Low Carbon Vehicle Technology Programme, which was funded by AWM-ERDF. The authors would like to acknowledge the LCVTP Work Stream 7 team members who have all made significant contributions to the work described herein – Dr Darren Hughes, Dr Mark Pharaoh, Dr Geraint Williams, Darren Stewardson, Dave Mossop, Nicholas Blundell, Prof Richard Dashwood, Dr Kerry Kirwan and the WMG LCVTP administrative team and our colleagues at Tata Motors European Technical Centre (TMETC, including Terry Wheeldon, Tony King and Mike Cromarty) and Jaguar-Land Rover.

11 Literature

[¹] Bandivadekar, A. E. A. “On The Road In 2035: Reducing Transportation's Petroleum Consumption And GHG Emissions”, *MIT Laboratory for Energy and the Environment, Cambridge, Massachusetts* (2008).

[²] Wohlecker, R., Johannaber, M. and Espig, M. “Determination of Weight Elasticity of Fuel Economy for ICE, Hybrid and Fuel Cell Vehicles”, *SAE World Congress & Exhibition, April 2007*. Detroit, MI, USA: SOCIETY OF AUTOMOTIVE ENGINEERS INC. (2007)

[³] WorldAutoSteel “Progress in Weight Loss Steel: Body Structures Keep the Slimming Trend Going” [Online]. http://www.worldautosteel.org/why-steel/mass-reduction/progress_vehicle_weight_loss/WorldAutoSteel. (2008) [Accessed 28-05-2012 2012].

[⁴] Lotus Engineering Inc. “An Assessment of Mass Reduction Opportunities for a 2017 – 2020 Model Year Vehicle Program”, *The International Council on Clean Transportation (ICCT)*, (2010)

[⁵] “TICONA Celstran® CFRT/LFRT Composites” [Online]. Available: http://www.ticona.com/home_page/homepage/beta_composites/beta_composites-celstran.htm [Accessed 3rd June 2012].

[⁶] LSTC “LS-DYNA Keywords Manual - Volume II: Material Models”, version 971, 2009

[⁷] K SCHWEIZERHOF, K. W., T MÜNZ, T ROTTNER, “Crashworthiness analysis with enhanced composite material models in LS-DYNA - Merits and Limits”. *5th International LS-DYNA User's Conference*. Detroit, 1998

[⁸] ASTM D3039 – “Standard Test Method for Tensile Properties of Polymer Matrix Composite Materials“

[⁹] ASTM D3518 – “Standard Test Method for In-Plane Shear Response of Polymer Matrix Composite Materials by Tensile Test of a $\pm 45^\circ$ Laminate“

[¹⁰] ASTM D2344/D2344M - 00(2006) “Standard Test Method for Short-Beam Strength of Polymer Matrix Composite Materials and Their Laminates“

[¹¹] CHAN, A., CHIU, W. K. & LIU, X. L. “Determining the elastic interlaminar shear modulus of composite laminates“. *Composite Structures*, 80, 2007 396-408.

[¹²] CHIAO, CC., „Measurement of shear properties of fibre composites“, *Journal of Composite Materials*, July 1977

[¹³] DAY, J., „Notes on MAT058“, [Online], <http://ftp.lstc.com/anonymous/outgoing/jday/composites/mat58>, [Accessed 15-01-2012]